Contact Dynamics Simulation of Rover Locomotion

Rainer Krenn, Andreas Gibbesch, Gerd Hirzinger
German Aerospace Center (DLR), Oberpfaffenhofen
rainer.krenn@dlr.de

Abstract

Software simulations of the locomotion play an important role in the chassis design and dimensioning phase of planetary rovers. In this paper two key modeling techniques for simulating the physical contact between rover wheels and planetary surface will be presented. The first one is PCM (Polygonal Contact Model). Generally, PCM provides the contact dynamics between two bodies, which are specified by polygonal surfaces and elastic surface layers. Here PCM is applied to the physical contact between wheels and hard rocks. The second one is SCM (Soil Contact Model) that represents the interaction between wheels and soft loose soil. SCM provides the dynamics of a plastically deformable surface using an elevation grid description. Both methods are prepared to be applied inside a multi-body simulation tool. The presented simulation results show two representative applications for the introduced contact dynamics models in terms of rover wheel drive design and multi-pass effect assessments.

1. Introduction

In the design phase of the rover chassis the simulation results of rover locomotion tests play an important role within the tradeoff of different chassis concepts. Due to the absence of applicable chassis hardware in early project phases and moreover, due to flexibility and adaptability reasons, e.g. consideration of specific gravity conditions on planets, software simulations are commonly preferred. However, the model fidelity regarding the interaction between the rover wheels or tracks and the planetary surface plays a crucial role since the accuracy and reliability of the simulation results influence strongly the tradeoff output.

Table 1: Stone Distribution (Mars, Viking I)

Class	Frequency
0.05 m	2 m^{-2}
0.1 m	1.7 m^{-2}
0.25 m	0.8 m^{-2}

For the design of the ExoMars rover chassis simulation results of rover locomotion inside a representative planetary terrain were required. Hereby a terrain based on measurements taken during Viking I mission [1] was defined as reference. It is described as a soil base with stones of different size classes and statistical distribution on top of the soil (see Table 1). In Figure 1 an example is given for a possible appearance of the terrain.

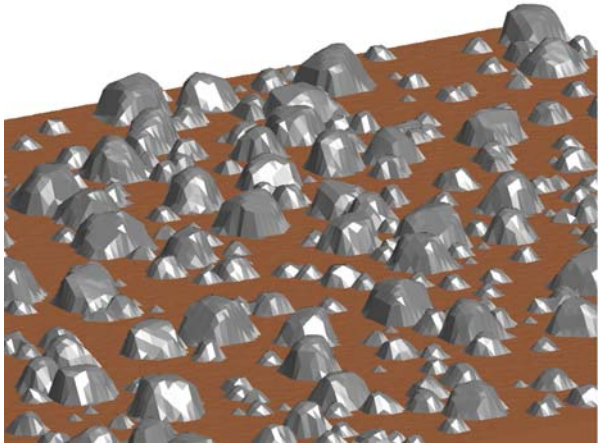

Figure 1: Virtual Reference Terrain

Therefore the simulation software should include contact dynamics models, which are able to deal with two completely different physical contact configurations: The contact of the metal wheel a) with hard rigid rocks and b) with plastic soil.

In the past a large number of various terra-mechanics based modeling and simulation approaches were presented. For the simulation of locomotion in sandy soil most of the authors apply the empirically found soil stress-strain laws as introduced by Bekker, e.g. [2] and Wong [3]. An according application for the motion analysis of planetary rovers was presented by Iagnemma et al.[4]. Alternatively a rheological soil model was proposed by Bolling [5]. Gibbesch et al. [6] implemented this model inside a multi-body simulation environment for rover mobility investigations. The model offers amongst others the investigation of multi-pass effects of a serious of wheels following the same track. Sophisticated FEM-inspired soil models are

presented by Grand et al. [7] focusing on the soil grain displacement beneath the wheel. An exemplarily approach for the development of a wheel-soil-interaction model based on experimental results could be found in [8] (Bauer et al.). Here, a single wheel test-bed was applied for an assessment of the wheel design. Ishigami, Yoshida et al. extended the single wheel setup to a full rover simulation with four steerable and controlled wheels [9]. Hereby, the complexity of the model was increased by taking into account lateral forces at the wheel. Poulakis et al. solved the simulation task for a six wheel rover on a wavy terrain using a bond graph based model description assuming single point contact of the wheels [10].

The goal of our new approach was to extend the state of the art of rover simulation such that a full 3D-simulation inside the reference terrain of Viking I will be possible by means of multi-body simulation methods. To reach this goal two major tasks had to be solved:

1) The implementation of a model for the interaction between hard rocks and the rover wheels: This contact problem can not be solved by applying the referenced terramechanics based approaches. However, an elegant solution of this problem was proposed by Hippmann [11] using the so-called Polygon Contact Model (**PCM**). The details are described in paragraph 2.1.

2) The implementation of a plastically deformable soil: Since FEM-methods are hardly applicable for multi-body dynamics formalisms the solution of this problem was inspired from computer graphics algorithms for terrain generation (e.g. Olsen [12]) and animating footprints in soil (e.g. Sumner et al. [13]). The specific implementation for the contact dynamics problem called Soil Contact Model (**SCM**) is documented in paragraph 2.2.

2. Modeling of Physical Contact

Since the nature of the two contact cases mentioned above (wheel-rock and wheel-soil) is completely different, two different models were implemented to be applied in parallel for the simulation of rover cruising on a planetary surface.

2.1. Contact between Wheels and Rocks

For the contact definition between wheels and rocks the so-called PCM (Polygon Contact Model, [11]) is used. For the body geometry definition a polygonal representation is used and the contact forces are determined by means of the elastic foundation model. This makes it possible to define contact between almost arbitrarily surfaces.

The surface model is based on the surface layer model, which can be developed from the half space approximation. The body interior is assumed to behave compliant to the rules of St. Venant. Additional dynamical effects due to accelerations during deformation are neglected. The principle of St. Venant adapted to contact definition in multi-body dynamics systems leads to the assumption that the contact stresses can be summed up and be taken into account as applied forces and torques. The deformation due to the impact is assumed to be small and therefore the bodies' center of mass and the inertia tensor remain constant. The half space approximation is valid for nearly homogeneous, isotropic and linear elastic bodies. The contact region should be small in comparison to the overall dimensions of the bodies. A comparison of these two approaches is shown in Figure 2. In contrast the surface layer method uses a rigid half space for both contact surfaces ($E = \infty$) with a linear elastic surface layer. The shear stresses are neglected and the correlation between sinkage and pressure in the same location can be written as:

$$u_n(x,y) = \frac{b}{K} \cdot p(x,y) \tag{1}$$

Therein b is the layer thickness and K the elastic modulus of the surface layer with

$$K = \frac{1-\nu}{(1+\nu)(1-2\nu)} \cdot E\,. \tag{2}$$

Reasonable results for the model can only be expected for values for the Poisson ratio of $\nu < 0.45$.

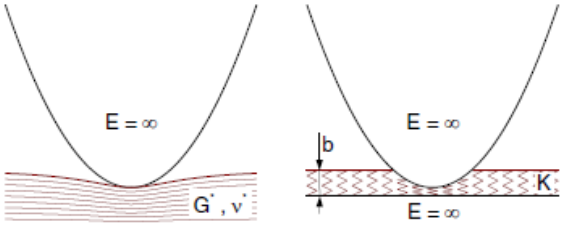

Figure 2: Comparison of Half Space Approximation (Left) and Surface Layer Model (Right)

Applying quasi-identical materials with $\kappa = 0$ the surface layer model is also valid for tangential contact modeling. The elastic material deviation κ is defined by

$$\kappa = \left(\frac{1-2\nu_1}{G_1} - \frac{1-2\nu_2}{G_2} \right) \frac{G^*}{4} \tag{3}$$

with

$$G^* = \frac{1}{\frac{1}{G_1} + \frac{1}{G_2}}. \tag{4}$$

Within PCM the elastic foundation model based on a discretization of the contact patch is implemented. Normal displacement and pressure are assumed to be constant within each triangular contact element. The normal of a contact element k of area A_k results to

$$F_{nk} = c_t \cdot A_k \cdot u_{nk} \tag{5}$$

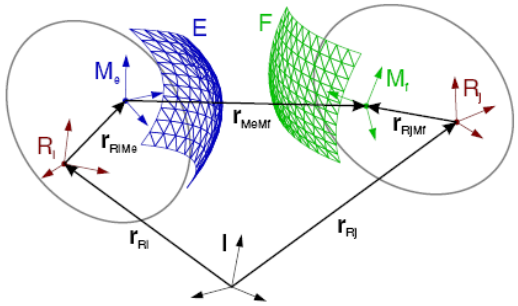

Figure 3: Kinematical Terms of a Contact Pairing

The PCM contact analysis task consists of three steps. First a collision detection algorithm determines if the contact pairing is in touch. If no collision is detected, the algorithm returns zero force and torque vectors and the analysis is finished. Otherwise PCM constructs in the second step the intersecting areas of the surfaces and discretizes the corresponding contact patches. Finally the contact force of each contact element is determined and the resulting contact force and torque of all contact elements is calculated.

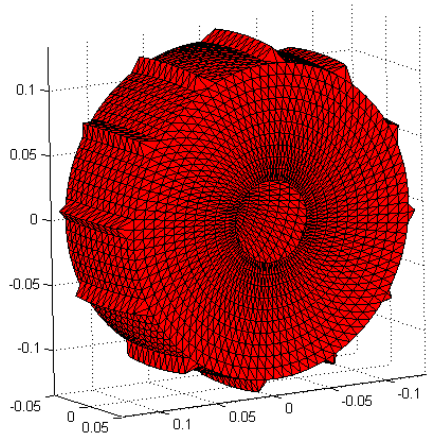

Figure 4: Polygonal Representation of Rover Wheel Used for PCM Contact Calculation

The collision detection is implemented by means of a highly efficient algorithm based on Bounding Volume (BV) hierarchies. The BV-algorithm reduces the number of costly triangle intersections tests with a factor of 10^4.

In Figure 4 and Figure 5 the polygonal representations of the contact bodies, wheel and soil of the Viking I terrain scenario are shown.

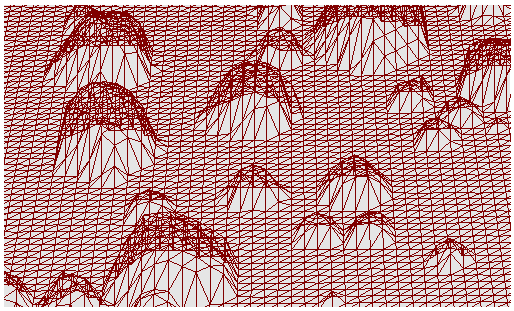

Figure 5: Polygonal Representation of Viking I Reference Terrain

2.2. Contact between Wheels and Plastic Soil

The contact problem wheel-soil can be generally described as the contact between a plastically deformable body and a rigid one. This implies that the elastic deformations of the rover wheels are negligible for the dedicated investigations. Therefore we have to focus on the soil model description.

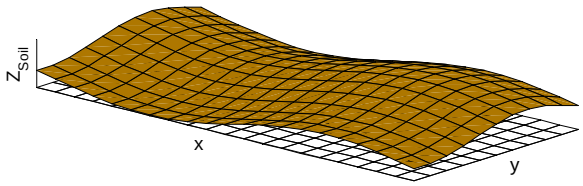

Figure 6: Soil Elevation Grid

2.2.1. Soil Surface Description

The soil surface inside the SCM algorithm is described as an elevation grid. It provides height information $Z_{Soil}\left(i_x, i_y\right)$ at discrete horizontal coordinates i_x and i_y, which are defined by a regular mesh grid of $n_x \cdot n_y$ nodes. The distances between adjacent grid nodes dxy are constant over the total surface. An example is given in Figure 6.

Beside the height information each grid node can be associated with a number of soil parameters and

deformation states. The most important individual attributes of the grid nodes are collected in Table 2.

Table 2: Soil Attributes of Grid Node

Parameters	
k_c	Cohesive modulus
k_φ	Frictional modulus
n	Exponent of sinkage
c	Cohesion
φ	Internal friction
States	
z	Plastic vertical soil deformation

2.2.2. Contact Detection between Wheel and Soil

Compared to PCM a BV-tree algorithm for contact detection is not required. SCM takes advantage of the fact that the soil is characterized as an elevation grid. Therefore contact can be easily and therefore very fast detected by comparing the z-coordinates of wheel surface vertices with the according soil elevation:

The wheel surface is originally described by n_V vertices ${}_{Wheel}\mathbf{V}$, which are expressed in the local wheel reference system,

$$ {}_{Wheel}\mathbf{V} = \begin{pmatrix} x_1 & y_1 & z_1 & 1 \\ x_2 & y_2 & z_2 & 1 \\ \vdots & \vdots & \vdots & \vdots \\ x_{n_V} & z_{n_V} & z_{n_V} & 1 \end{pmatrix}. \tag{6} $$

Assuming the pose transformation $\mathbf{B}$ (homogeneous transformation matrix) from the soil reference frame to the wheel reference frame with

$$ \mathbf{B} = \begin{pmatrix} \mathbf{A} & \mathbf{R} \\ \mathbf{0} & 1 \end{pmatrix} = \begin{pmatrix} A_{xx} & A_{yx} & A_{zx} & R_x \\ A_{xy} & A_{yy} & A_{zy} & R_y \\ A_{xz} & A_{yz} & A_{zz} & R_z \\ 0 & 0 & 0 & 1 \end{pmatrix}, \tag{7} $$

we can express the wheel vertices in the soil reference system by

$$ {}_{Soil}\mathbf{V} = {}_{Wheel}\mathbf{V} \cdot \mathbf{B}^T . \tag{8} $$

Now we are able to identify the according soil node by calculating the grid coordinates with

$$ i_x = (\mathrm{int})\frac{{}_{Soil}V_x}{dxy},\ i_y = (\mathrm{int})\frac{{}_{Soil}V_y}{dxy} \tag{9} $$

and to check for contact/no contact as follows:

$$ z(i_x, i_y) = Z_{Soil}(i_x, i_y) - {}_{Soil}V_z \begin{cases} > 0 \Rightarrow \text{contact} \\ < 0 \Rightarrow \text{no contact} \end{cases}. \tag{10} $$

Since usually more than one wheel vertices are projected onto one unique soil grid node, the $n_{Contact}$ vertices with minimum height respectively have to be defined as the contact vertices ${}_{Wheel}\mathbf{V}_{Contact}$.

As long as the distances of adjacent surface vertices at the wheel are smaller than the grid node distances of the soil the algorithm works well without any knowledge of the wheel surface polygons.

2.2.3. Contact Kinematics

Once the contact is detected the relative kinematics between wheel and soil at the according contact point $i_{Contact}$ can be calculated. The vertex velocity expressed in the soil reference system reads as follows:

$$ \mathbf{v}_{Contact} = \mathbf{v}_{Wheel} + \boldsymbol{\omega}_{Wheel} \times \left(\mathbf{A} \cdot {}_{Wheel}\mathbf{V}(i_{Contact}) \right) \tag{11} $$

Herein, $\mathbf{v}_{Wheel}$ and $\boldsymbol{\omega}_{Wheel}$ are the absolute linear and angular velocities of the wheel reference frame. In order to obtain the contact penetration velocity the gradient of the soil surface and the surface normal vector $\mathbf{n}$ has to be taken into account. With the discrete soil surface description the according tangent vectors can be expressed by vectors between adjacent soil surface points in x- and y-direction:

$$ \frac{\partial_{Soil} Z}{\partial x}(i_x, i_y) = \begin{pmatrix} dx \\ 0 \\ \dfrac{{}_{Soil}Z(i_x+1, i_y) - {}_{Soil}Z(i_x-1, i_y)}{2} \end{pmatrix} \tag{12} $$

$$ \frac{\partial_{Soil} Z}{\partial y}(i_x, i_y) = \begin{pmatrix} 0 \\ dy \\ \dfrac{{}_{Soil}Z(i_x, i_y+1) - {}_{Soil}Z(i_x, i_y-1)}{2} \end{pmatrix} $$

And following the normal vector is the results of

$$ \mathbf{n} = \frac{\partial_{Soil} Z}{\partial x} \times \frac{\partial_{Soil} Z}{\partial y}. \tag{13} $$

Now the tangent vector $\mathbf{t}$ in terms of $\mathbf{v}_{Contact}$ is defined as well:

$$ \mathbf{t} = \mathbf{n} \times \frac{\mathbf{n} \times \mathbf{v}_{Contact}}{|\mathbf{n} \times \mathbf{v}_{Contact}|} \tag{14} $$

The lengths of the vectors $\mathbf{n}$ and $\mathbf{t}$ are both equal to the size of the discrete soil surface area. The projection of $\mathbf{v}_{Contact}$ onto $\mathbf{n}$,

$$ \mathbf{v}_{Normal} = \left(\mathbf{v}_{Contact}^T \mathbf{n}_0 \right) \cdot \mathbf{n}_0; \quad \mathbf{n}_0 = \frac{\mathbf{n}}{|\mathbf{n}|}, \tag{15} $$

and onto $\mathbf{t}$,

$$ \mathbf{v}_{Tangential} = \left(\mathbf{v}_{Contact}^T \mathbf{t}_0 \right) \cdot \mathbf{t}_0; \quad \mathbf{t}_0 = \frac{\mathbf{t}}{|\mathbf{t}|}. \tag{16} $$

will be applied for force calculations in the following paragraphs.

2.2.4. Contact Dynamics and Applied Forces

With the prerequisites introduced in the previous paragraphs we are now able to calculate the soil pressure p at a discrete surface grid node applying the sinkage-pressure relation according to Bekker:

$$p = \left(\frac{k_c}{b} + k_\varphi \right) z^n . \tag{17}$$

Herein b is interpreted as the width of the penetrating wheel. Then, the applied normal force $\mathbf{F}_{normal}$ can be immediately expressed by

$$\mathbf{F}_{normal} = p\mathbf{n} . \tag{18}$$

The implementation of the tangential forces $\mathbf{F}_{tangential}$ is compliant with the Coulomb rule for the adhesion between wheel surface and soil surface with the friction coefficient μ:

$$\mathbf{F}_{tangential} = \mu p\mathbf{t} . \tag{19}$$

Now, the force and torque applied to one discrete contact vertex $i_{Contact}$ and expressed in the wheel reference frame can be calculated as follows:

$$\mathbf{F}\left(i_{Contact}\right) = \mathbf{A}^T \cdot \left(\mathbf{F}_{normal}\left(i_{Contact}\right) + \mathbf{F}_{tangential}\left(i_{Contact}\right) \right) \tag{20}$$

$$\mathbf{T}\left(i_{Contact}\right) = {}_{Wheel}\mathbf{V}_{Contact}\left(i_{Contact}\right) \times \mathbf{F}\left(i_{Contact}\right) \tag{21}$$

The total applied force and torque is then the discrete integral over the total contact area of $n_{Contact}$ contact vertices:

$${}_{Weel}\mathbf{F} = \sum_{i_{Contact}=1}^{n_{Contact}} \mathbf{F}\left(i_{Contact}\right), \quad {}_{Weel}\mathbf{T} = \sum_{i_{Contact}=1}^{n_{Contact}} \mathbf{T}\left(i_{Contact}\right). \tag{22}$$

2.2.5. Plastic Deformation of Soil

The implementation of a plastically deformable soil into the contact model was motivated by the rover simulation task. While cruising we have the leading rover wheels, driving through untouched soil with a significant drawbar pull while the wheels following inline can drive into the pre-compressed soil at completely different rolling resistance (multi-pass). Moreover, it should be possible to simulate self-carving of the wheels into the soil under adverse conditions.

A further motivation is caused by the nature of the elevation grid based soil model. Herein a classical shear stress – shear deformation relation according to Janosi and Hanamoto [14] is hardly implementable since only vertical degrees of freedom are provided by the soil model. On the other hand, shear deformations are always connected with vertical penetrations of contact objects. In this process the contact shape normal vectors obtain horizontal components, which provide in connection with the sinkage pressure the required shear forces (see (18)) in a consistent system without additional empirical equations.

The plastic soil deformation algorithm is inspired by computer graphics solutions and consists of three steps:

1) The displacement of soil volume from the contact penetration area: Supposing an incompressible soil the total amount of displaced soil is equal to the intersection volume of wheel surface and the initial soil surface. This implies that the soil height reduction ΔZ_{Soil} is equal to the wheel sinkage z at the according grid node. The displaced volume D at one discrete contact grid node $\left(i_x, i_y\right)$ can be calculated with (10) by

$$D\left(i_x, i_y\right) = \Delta Z_{Soil}\left(i_x, i_y\right) \cdot dxy \cdot dxy . \tag{23}$$

2) The temporary deposition of the displaced soil at the boarder of the contact area: In this step for each contact grid node the volume D will be distributed to the boarder grid nodes reciprocally proportional to their distances to the contact grid nodes. The individual weighting factor w for a boarder grid node with respect to a contact grid node will be calculated as follows:

$$w = \frac{1}{\left(i_{x,Boarder} - i_{x,Contact}\right)^2 + \left(i_{y,Boarder} - i_{y,Contact}\right)^2} . \tag{24}$$

An example for soil displacement and temporary deposition is given in Figure 7. Here a wheel was rolling over the soil with a constant declination, respectively with a continuously raising sinkage.

3) The erosion of the temporarily deposed soil volume: When sand is piled a maximum sand hill slope angle φ can be achieved due to internal friction of the sand. Therefore after deposition of the removed soil volume an erosion algorithm will be applied to the soil grid nodes in the vicinity of the contact area. In this process the erosion potential of an investigated grid node $\left(i_x, i_y\right)$ to its four adjacent grid nodes $\left(i_x \pm 1, i_y \pm 1\right)$ is being defined by the according height differences dZ:

$$dZ_{1,2,3,4} = \left(Z_{Soil}\left(i_x, i_y\right) - Z_{Soil}\left(i_x \pm 1, i_y \pm 1\right) \right) . \tag{25}$$

Then, the actual erosion depends on the maximum potential

$$dZ_{\max} = \max\left(dZ_{1,2,3,4}\right) . \tag{26}$$

If this amount exceeds the limit dZ_{Limit} defined by

$$dZ_{Limit} = dxy \cdot \tan\varphi \tag{27}$$

the erosion ΔZ_{Soil} to the adjacent grid nodes takes place as follows:

$$\Delta Z_{Soil}\left(i_x, i_y\right) = -\frac{dZ_{\max} - dZ_{Limit}}{2}$$
$$\Delta Z_{Soil}\left(i_x \pm 1, i_y \pm 1\right) = +\frac{dZ_{\max} - dZ_{Limit}}{2} \cdot \frac{dZ_{1,2,3,4}}{\sum_{i=1}^{4} dZ_i} \qquad (28)$$

Herein it is expressed that half of the excess height is being removed from the investigated grid node and added to the neighbor nodes according to their individual fraction of the total erosion potential. An example for an actual result of plastic soil deformation including erosion is given in Figure 8. Hereby the same wheel trajectory was performed as for Figure 7, but without freezing the intermediate deposition state.

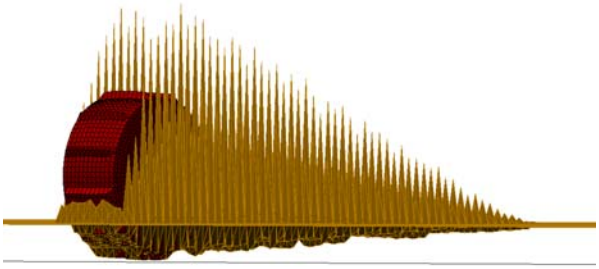

Figure 7: Soil Displacement and Temporary Deposition without Erosion

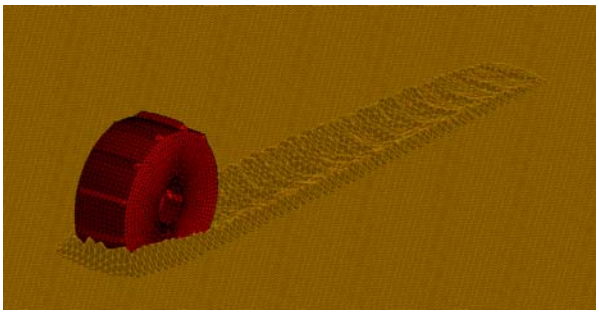

Figure 8: Soil Displacement, Deposition and Erosion

2.2.6. Adaptation of Pressure – Sinkage Function

In (17) the wheel sinkage- soil pressure– function was introduced for a non-deformed soil surface. For the implementation into SCM the soil deformation, respectively the pre-compression of the soil has to be taken into account. Therefore function (17) is extended by a sinkage correction z_0:

$$p = \left(\frac{k_c}{b} + k_\varphi\right)\left(z + z_0\right)^n; \quad 0 \le z_0 < \infty. \qquad (29)$$

Since z_0 is the accumulative sum of all successive soil deformations ΔZ_{Soil} it guarantees for the continuity of the soil pressure while removing soil from the contact area and for the correct reduction of the pre-compression outside the contact zone when soil will be deposed there.

3. Simulation Results

In the following paragraph two examples for possible applications of PCM and SCM for planetary rover simulations are presented.

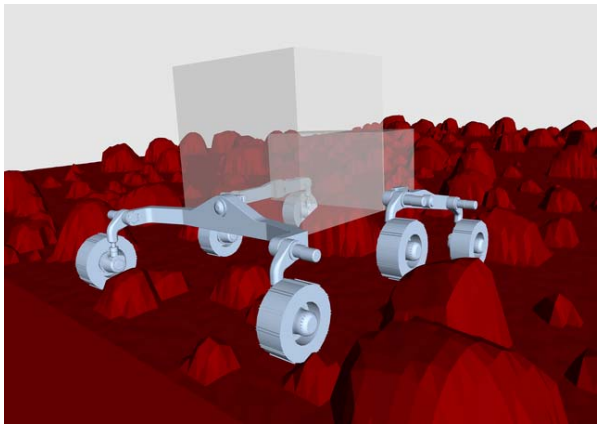

Figure 9: MBS Model of Exomars Rover on Rocky Mars Reference Terrain

A number of PCM simulation results of a rover on rocky terrain (shown in Figure 9) are depicted in Figure 10 and Figure 11. Therein the actuator and steering torques for all six wheels are shown for the rover driving through this typical scenario with an average speed of about 7m/15min.

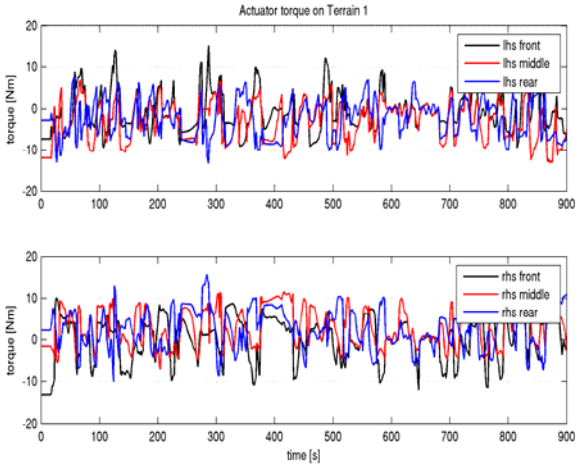

Figure 10: Rover actuator torque

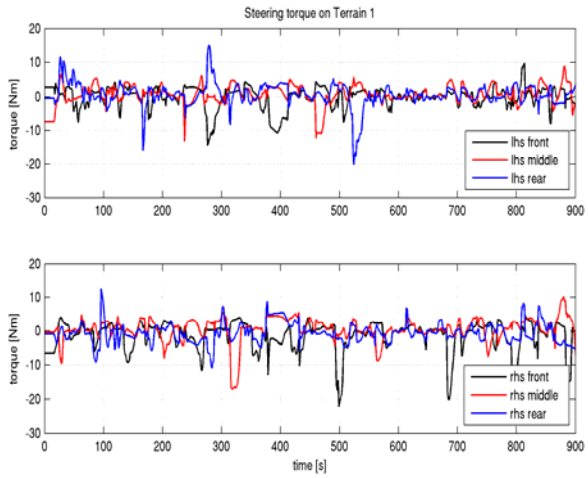

Figure 11: Rover steering torque

The goal of the according simulation campaign was the assessment of the required actuator power to be installed in the drives of the ExoMars rover.

A completely different kind of simulation results is presented as example for an SCM application. Here the multi-pass effect of wheel pairs rolling inline was investigated (Figure 12).

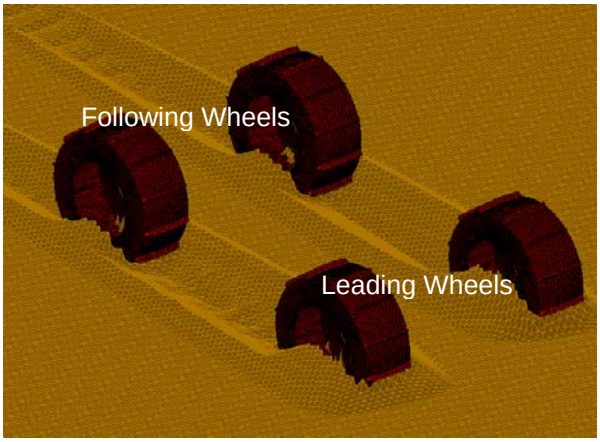

Figure 12: Wheel Configuration for Multi-Pass Investigation

The following plot figures show the applied forces onto the rolling wheels. The rheonomical trajectories of the wheel axes with a given declination have caused a continuous sinkage of the wheels into the soil during rolling. In Figure 13 and Figure 14, the diagrams 1 and 3 show the force impact on the leading wheels while diagrams 2 and 4 show the according values of the wheels following the tracks of the leading ones. The time axes of the diagrams are arranged in a way that the impact on the leading and following wheels can compared directly.

The first simulation was performed assuming completely loose and incompressible soil with 100% displacement soil from the sinkage volume of the wheels (see Figure 13). Here the multi-pass effect in terms of force reduction is negligible since the soil displaced from the leading wheels flows back into the track and therefore the wheels following inline have to roll against a similar drawbar pull as the leading ones.

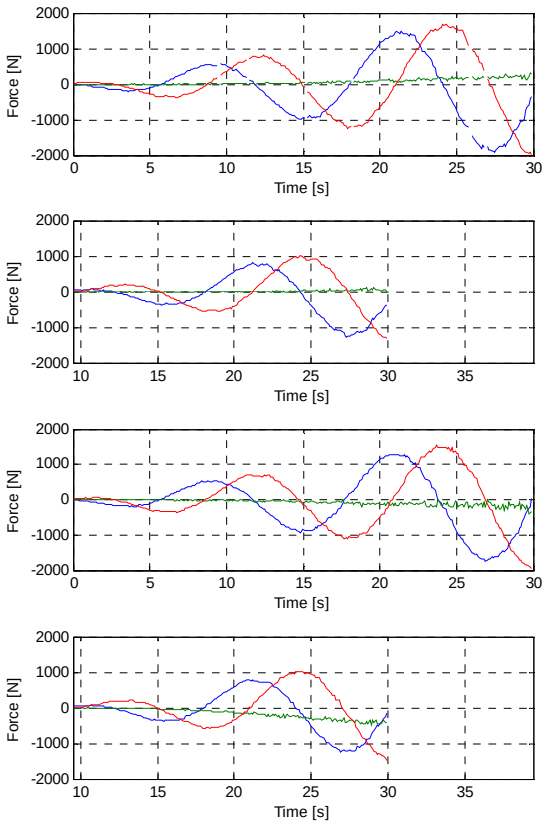

Figure 13: Multi-Pass Investigation within Incompressible Loose Soil (Wheel Forces: Red/Blue = Radial, Green = Axial)

In opposite to those results obtained for incompressible loose soil the effects of multi-pass can be clearly detected within the results for compressible soil. In Figure 14 the according results for 50% soil compression and 50% soil displacement are presented. Here we can state that the rolling resistance for the following wheels is significantly lower caused by the reduced drawbar pull. Moreover, in Figure 14, diagrams 2 and 4 we can identify the influences of the grousers, which is indicated by the superposed oscillations of the forces.

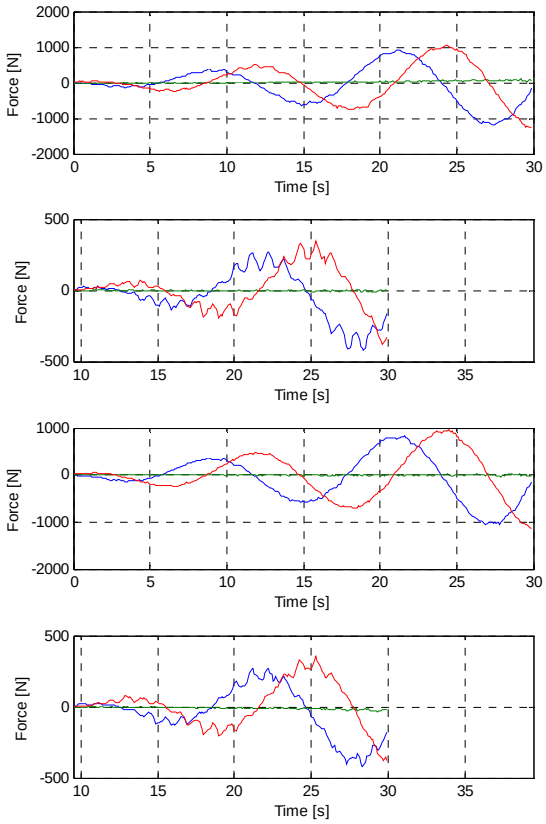

Figure 14: Multi-Pass Investigation within Compressible Soil (Wheel Forces: Red/Blue = Radial, Green = Axial)

4. Conclusion

In this paper two models for the simulation of the wheel-soil interaction in different kind of terrain conditions were introduced. Currently both are applied for specific kind of simulations as documented in chapter 3. In future work both methods will be combined in order to significantly enlarge the capabilities and reliability of the rover locomotion simulation by means of multi-body simulation tools.

5. References

[1] M.Golombek and D. Rapp, *Size frequency distributions of rocks on Mars and Earth analog sites*, Journal of Geophysical Research, 102(E2), pp 4117-4129, 25 February 1997

[2] M.G. Bekker, *Introduction to Terrain-Vehicle Systems*, The University of Michigan Press, Ann Arbor, USA, 1969.

[3] J.Y. Wong. *Theory of Ground Vehicles*, Wiley, New York, 3rd Edition, 2001.

[4] K. Iagnemma and S. Dubowsky, *Mobile Robots in Rough Terrain - Estimation, Motion Planning, and Control with Application to Planetary Rovers*, Springer Tracts in Advanced Robotics, Volume 12, Springer, Berlin, 2004.

[5] I. Bolling. *Bodenverdichtung und Triebkraftverhalten bei Reifen - Neue Meß- und Rechenmethoden*, Dissertation, TU München, 1987.

[6] A. Gibbesch and B. Schäfer. *Modelling of planetary rovers by means of a dynamical system approach with respect to mobility requirements*, 10th European Conference of the ISTVS 2006, Budapest, Hungary, 3-6 October 2006.

[7] C. Grand, F. Ben Amar, P. Bidaud and G. Andrade, *A simulation system for behaviour evaluation of off-road mobile robots*, 4th Int. Conference on Climbing and Walking Robots (CLAWAR), Karlsruhe, Germany, 24-26 September 2001

[8] R. Bauer, W. Leung and T. Barfoot, *Experimental and Simulation Results of Wheel-Soil Interaction for Planetary Rovers*, IROS 2005, Edmonton, Alberta, Canada, 2-6 August 2005

[9] G. Ishigami, A. Miwa, K. Nagatani and K. Yoshida, *Terramechanics-Based Model for Steering Maneuver of Planetary Exploration Rovers on Loose Soil*, Journal of Field Robotics 24(3), pp 233-250, Wiley InterScience, 2007

[10] P. Poulakis, L. Joudrier, S.Stramigioli, *Modeling and Simulation of Planetary Rover Locomotion on Rough Terrain: Implementation in 20-sim*, 9th Int. Workshop on Simulation for European Space Programmes, SESP 2006, ESA/ESTEC, Noordwijk, The Netherlands, 6-8 November 2006

[11] G. Hippmann, *Modellierung von Kontakten komplex geformter Körper in der Mehrkörpersimulation*, Dissertation, TU Wien, 2004.

[12] J. Olsen, *Realtime Procedural Terrain Generation*, IMADA, University of Southern Denmark, 31 October, 2004

[13] R.W. Sumner, J.F. O´Brien and J.K. Hodgins, *Animation Sand, Mud and Snow*, Computer Graphics Forum, Volume 18, No 1, 1999

[14] Z. Janosi and B. Hanamoto, Analytical Determination of Drawbar Pull as a Function of Slip for Tracked Vehicles in Deformable Soils, 1st Int. Conference on Terrain-Vehicle Systems, Turin, Italy, 1961